

Stereographical visualization of a polarization state using weak measurements with an optical-vortex beam

Hirokazu Kobayashi,^{1,*} Koji Nonaka,¹ and Yutaka Shikano^{2,3,†}

¹*Department of Electronic and Photonic System Engineering,
Kochi University of Technology, Tosayamada-cho, Kochi, Japan.*

²*Research Center of Integrative Molecular Systems (CIMoS),
Institute for Molecular Science, Okazaki, Aichi, Japan.*

³*Institute for Quantum Studies, Chapman University, Orange, California 92866, USA.*

(Dated: October 2, 2018)

We propose a stereographical-visualization scheme for a polarization state by two-dimensional imaging of a weak value with a single setup. The key idea is to employ Laguerre–Gaussian modes or an optical vortex beam for a probe state in weak measurement. Our scheme has the advantage that we can extract information on the polarization state from the single image in which the zero-intensity point of the optical vortex beam corresponds to a stereographic projection point of the Poincaré sphere. We experimentally perform single-setup weak measurement to validate the stereographical relationship between the polarization state on the Poincaré sphere and the location of the zero-intensity point.

PACS numbers: 03.65.Wj, 42.50.Xa, 42.30.Wb

I. INTRODUCTION

Weak measurement was originally proposed by Aharonov, Albert, and Vaidman [1] as an extension to the standard von Neumann model of quantum measurement, inspired by the two-state vector formalism of quantum mechanical measurement [2]. This formalism is characterized by the pre- and post-selected states of the measured system. In contrast to an ideal (strong) measurement, weak measurement extracts very little information about the measured system from a single outcome, but the measured state does not collapse. Although each outcome of weak measurement includes a large uncertainty, the averaged value in multiple trials can build up a significant value, called a weak value, without state collapse. This feature makes weak measurement an ideal tool for examining the fundamentals of quantum physics, such as quantum correlation and quantum dynamics; for instance, see the reviews [3–7].

On the basis of the above property, recent works have theoretically shown that weak measurement can be used for observing the quantum wavefunction [8–12]. In contrast to conventional quantum-state tomography [13], this scheme records the complex-valued weak values describing the wavefunction of the quantum state and requires less post-processing. Recently, Lundeen and his colleagues demonstrated weak measurement of the one-dimensional transverse wavefunction [14]. Since then, state tomography via weak measurement has been applied to several physical systems, such as an average photon trajectory [15, 16], a polarization state [17], and an orbital angular momentum state [18]. All of these demon-

strations, however, require the experimental configuration to measure two noncommutative operators, such as a position operator \hat{X} and its momentum operator \hat{P}_x , onto the probe state of the weak measurement.

In this paper, we propose a stereographical-visualization scheme for a polarization state by two-dimensional imaging of the weak value with two commutative position operators. The key idea is to employ Laguerre–Gaussian (LG) modes for a probe state in weak measurement, and it weakly interacts with the measured polarization state, as proposed in Refs. [19, 20]. The LG mode has a zero-intensity point (ZIP) in the center, which is generally called an *optical vortex* [21], and several generation methods have been proposed and demonstrated [22–30]. Note that the relationship between the optical vortex beam and the weak value has been pointed out from different viewpoints [31–35]. According to Refs. [19, 20], we can extract information on the polarization state from a single image as the two-dimensional location of the ZIP, which corresponds to the stereographic projection point of the polarization state on the Poincaré sphere. We also experimentally verify the stereographical relationship between the polarization state and the location of the ZIP. Furthermore, this is a practical demonstration of weak measurement using an optical vortex beam as the probe state.

The remainder of this paper is organized as follows. In Sec. II, we show the stereographical relationship between a polarization state on the Poincaré sphere and a weak value of a polarization state and propose a stereographical-visualization scheme for the polarization state by using the weak measurement with an optical vortex beam. In Sec. III, we experimentally implement our scheme by using a polarizing Sagnac interferometer including a specialized half-wave plate, called q plate. We demonstrate our proposed scheme and evaluate its accuracy from the fidelity of the measurement results. Sum-

*Electronic address: kobayashi.hirokazu@kochi-tech.ac.jp

†Electronic address: yshikano@ims.ac.jp

mary and discussion are presented in Sec. IV.

II. STEREOGRAPHICAL VISUALIZATION OF A QUBIT STATE

Let us consider the geometrical relationship between a weak value and a two-dimensional quantum (qubit) state. Let any qubit state $|\psi\rangle$ spanned by orthonormal basis states $|0\rangle$ and $|1\rangle$ be denoted as

$$|\psi\rangle = \cos\theta|0\rangle + e^{i\phi}\sin\theta|1\rangle, \quad (1)$$

where $0 \leq \theta \leq \frac{\pi}{2}$, and $0 \leq \phi < 2\pi$. Here, the parameters ϕ and θ uniquely specify a point on the unit sphere S^2 , called the Bloch sphere, which is the same as the Poincaré sphere in optics, in which the states $|0\rangle$ and $|1\rangle$ correspond to the north and south poles, respectively. We consider the weak value of the observable $\hat{\sigma}_x \equiv |0\rangle\langle 1| + |1\rangle\langle 0|$, which is the x component of the Pauli matrices, with the post-selected state $|1\rangle$:

$$\langle \hat{\sigma}_x \rangle_w \equiv \frac{\langle 1|\hat{\sigma}_x|\psi\rangle}{\langle 1|\psi\rangle} = \frac{\langle 0|\psi\rangle}{\langle 1|\psi\rangle} = e^{-i\phi} \cot\theta, \quad (2)$$

which is generally a complex value. This weak value gives a geometrical mapping of the qubit state on the Bloch sphere, namely, the stereographic projection, as shown in Fig. 1.

The stereographic projection is one way to make a flat map of a spherical surface. Let $P(|0\rangle)$ denote the north pole on the Bloch sphere. Given a point $P(|\psi\rangle)$ related to the qubit state $|\psi\rangle$, other than $P(|0\rangle)$, the line connecting $P(|0\rangle)$ and $P(|\psi\rangle)$ intersects a certain flat complex (two-dimensional real) plane orthogonal to the line connecting $P(|0\rangle)$ and $P(|1\rangle)$ at exactly one point, $G\psi \equiv G(\text{Re}\langle \hat{\sigma}_x \rangle_w, \text{Im}\langle \hat{\sigma}_x \rangle_w)$. Thus, the stereographic projection can be taken as the map $\pi : S^2 - P(|0\rangle) \rightarrow \mathbb{C} \simeq \mathbb{R}^2 : P(|\psi\rangle) \rightarrow G\psi$. From a geometrical viewpoint, it is easily understood that the stereographically

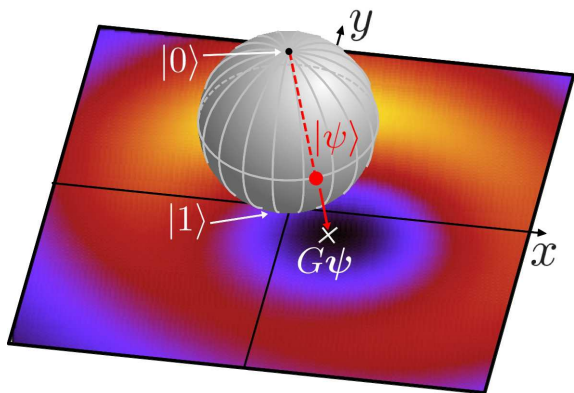


FIG. 1: Stereographic projection of qubit state $|\psi\rangle$ on Bloch sphere to the ZIP, $G\psi = G(\text{Re}\langle \hat{\sigma}_x \rangle_w, \text{Im}\langle \hat{\sigma}_x \rangle_w)$. As an example, the $l = 1$ case is illustrated.

projected point corresponding to the weak value can become far from the origin of the complex plane. The south pole $P(|1\rangle)$ appears at the origin of the complex plane. Lines of latitude appear as circles around this origin. The southern hemisphere of the Bloch sphere is not stretched very much in the map, but the northern hemisphere is stretched quite a bit, and the north pole is at infinity.

To extract the real and imaginary parts of the weak value from a single image, we can use the LG mode as the probe state [19, 20]. The LG mode is one of the natural solutions of the paraxial wave equation and is characterized by a radial index p and an azimuthal index l . The modes have an annular intensity distribution around the ZIP. The wavefront of the LG modes is composed of $|l|$ intertwined helical wavefronts, with a handedness given by the sign of l . In what follows, we consider the optical vortex beam with $p = 0$ and $l > 0$ for simplicity.

The amplitude distribution of the LG mode is given as

$$\begin{aligned} \phi_i(x, y) &= \langle x, y|\phi_i\rangle \\ &\propto f_l(x, y) \exp\left(-\frac{x^2 + y^2}{4W_0^2}\right), \end{aligned} \quad (3)$$

where W_0 corresponds to the beam width, and $f_l(x, y) \equiv (x+iy)^l$ determines the ZIP as the origin. Unlike a fundamental Gaussian mode ($l = 0$), the LG mode is no longer factorable in two directions, x and y , and this is a key factor for retrieving the real and imaginary parts of the weak value from a single image. To apply the weak measurement scheme, we use the von Neumann interaction Hamiltonian,

$$\hat{H} = g\delta(t - t_0)\hat{\sigma}_x \otimes \hat{P}_x, \quad (5)$$

where the coupling constant g is sufficiently small, and \hat{P}_x is the momentum observable on the probe system conjugate to the commuting position observable \hat{X} . For simplicity, we assume the interaction to be impulsive at time $t = t_0$. After the interaction between the system state and the LG mode probe states, we post-select the system in $|1\rangle$, resulting in the probe state described as

$$\begin{aligned} |\phi_f\rangle &= \langle 1|e^{-iG\hat{\sigma}_x \otimes \hat{P}_x}|\psi_i\rangle|\phi_i\rangle \\ &\simeq \langle 1|\psi_i\rangle \exp\left(-iG\langle \hat{\sigma}_x \rangle_w \hat{P}_x\right) |\phi_i\rangle \end{aligned} \quad (6)$$

with $G \equiv g/\hbar$. Note that this approximation is justified under the condition

$$\frac{W_0}{G} \gg \max(1, |\langle \hat{\sigma}_x \rangle_w|). \quad (7)$$

Without this condition, the exact calculation can be described (see Appendix A). From Eq. (6), the spatial intensity distribution of the probe state after post-selection can be calculated as

$$\begin{aligned} |\phi_f(x, y)|^2 &\propto |\phi_i(x - G\langle \hat{\sigma}_x \rangle_w, y)|^2 \\ &\propto |f_l(x - G\text{Re}\langle \hat{\sigma}_x \rangle_w, y - G\text{Im}\langle \hat{\sigma}_x \rangle_w)|^2 \\ &\times \exp\left[-\frac{(x - G\text{Re}\langle \hat{\sigma}_x \rangle_w)^2 + y^2}{2W_0^2}\right]. \end{aligned} \quad (8)$$

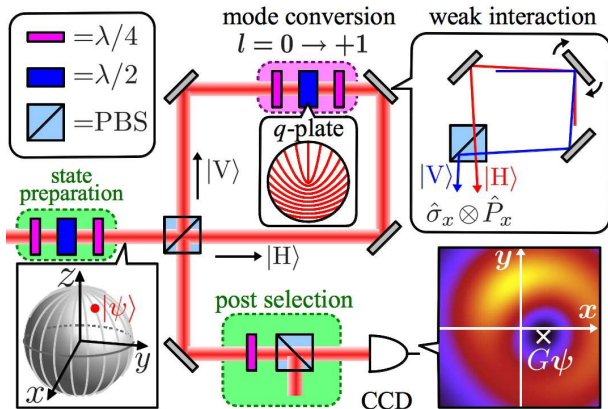


FIG. 2: Experimental setup with the polarizing Sagnac interferometer.

Therefore, the ZIP is shifted by the real and imaginary parts of the weak value $\langle \hat{\sigma}_x \rangle_w$ in the two-dimensional image. Consequently, we can determine the qubit state on the Bloch sphere from the ZIP related to the stereographic projection, as shown in Fig. 1.

It is remarkable that our scheme can be generalized to the mixed state case, in which the qubit state is inside the Bloch sphere. The above procedure is applied to different post-selected states, e.g., $|0\rangle$, $(|0\rangle + i|1\rangle)/\sqrt{2}$, and $(|0\rangle - i|1\rangle)/\sqrt{2}$. Then, we can always choose at least two imaging planes to satisfy the approximation condition (7). From the two ZIPs, we can find the crossing point on the stereographic projection, which is the qubit state in the mixed state case. According to Refs. [36, 37], we need to prepare at least four imaging planes for any unknown qubit state.

III. EXPERIMENT BY WEAK MEASUREMENT WITH LAGUERRE-GAUSSIAN MODES

Figure 2 shows our experimental setup for demonstrating direct mapping of the polarization state onto the ZIP. We use a fiber-pigtailed continuous-wave laser with a wavelength of 785 nm, a power of 5 mW, and a beam waist radius of 1 mm. First, we prepare the fundamental Gaussian beam ($l = 0$) with an arbitrary polarization state using half-wave plates and quarter-wave plates in the state preparation stage. Next, we convert the spatial mode to the LG mode using a specially fabricated wave plate called a q plate [27]. The q plate has a suitably patterned transverse optical axis to couple the photon spin (polarization) with its orbital angular momentum [27]. Here, we use a q plate (Altechna, RPC-800-6) with a singularity charge $q = 1/2$ and uniform birefringent retardation $\delta = \pi$. This q plate can modify the mode number l to $l \pm 1$, the sign of which depends on the input polarization. The helicity of the output circular polarization

is also inverted.

To implement the above mode conversion without changing the output polarization, we propose a mode conversion setup based on a polarizing Sagnac interferometer (PSI) including the q plate. This setup ideally is 100% efficient for mode conversion and has good stability because of self-compensation of the optical paths inside the interferometer. The incident polarization remains unchanged because of the same optical path in the right-circulating and left-circulating paths inside the interferometer. A single polarizing beam splitter (PBS) is used as the entry and exit gates of the device. The PBS splits the incident beam into its horizontal component $|H\rangle \equiv (|0\rangle + |1\rangle)/\sqrt{2}$ and its vertical component $|V\rangle \equiv (|0\rangle - |1\rangle)/\sqrt{2}$, which circulate inside the interferometer along the same path, but in opposite directions. The spatial mode of each polarization component is converted to the LG mode with $l = 1$ by using quarter-wave plates with an angle of 45° and the q plate. After being reflected by the mirrors, they recombine again and exit the interferometer from the other side of the PBS. After passing through the interferometer, the two counter-propagating orthogonal polarizations $|H\rangle$ and $|V\rangle$ gain the same optical length. In this way, our setup can convert the incident fundamental Gaussian mode ($l = 0$) into the LG mode ($l = 1$) without a polarization change.

Inside the PSI, the weak interaction is obtained by slightly tilting the mirror of the PSI as expressed in Eq. (5). After it passes through the PSI, we post-select the polarization state into the right circular polarization basis $|R\rangle \equiv |1\rangle$ and observe the spatial intensity distribution using a CCD image sensor with a pixel size of $6.45 \mu\text{m}$. Recall that our setup differs from the measurement interaction of the optical paths in the Sagnac interferometer [38]. Note also that this extends previous experimental studies on weak measurement of the polarization [39, 40].

Figure 3 shows our experimental results. Figures 3(a) and 3(c) show experimental setups to prepare the polarization states. Figures 3(b) and 3(d) depict the observed intensity distribution (inset figures), estimated polarization states from the weak measurement (red points), and the theoretical path of prepared polarization states (blue dashed line). First, we observed the linear polarization states around the equator on the Poincaré sphere, as shown in Fig. 3(a) and 3(b). We can confirm that the ZIP represented by the white cross in Fig. 3(b) moves along the circle corresponding to the equator on the Poincaré sphere. Next, we observed the polarization states along the more complex path, namely, the ∞ -shaped path on the southern hemisphere of the Poincaré sphere. The ∞ -shaped path is realized by using two quarter-wave plates, one of which is rotated and the other of which is fixed at an angle of 45° with respect to the direction of the input linear polarization [see Fig. 3(c)]. We can see that the experimentally-obtained ZIP moves along the ∞ -shaped path, as shown in Fig. 3(d). These experimental results indicate that the polarization states can

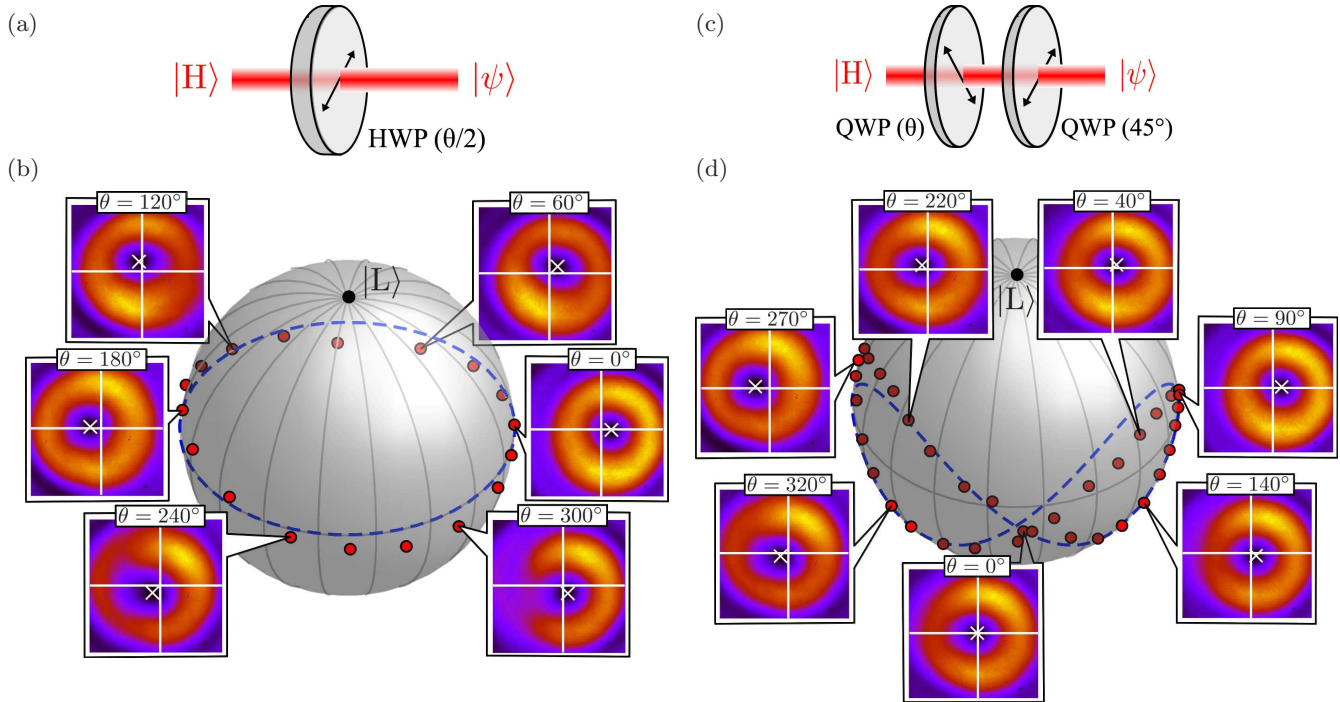


FIG. 3: Experimental observation of ZIP related to the stereographic projection of the polarization states around (a),(b) the equator and (c),(d) the ∞ -shaped path of the southern hemisphere on the Poincaré sphere. (a), (c) Experimental setup for state preparation. (b), (d) Theoretical path of prepared polarization states (blue dashed line) and experimentally-obtained polarization states from the weak measurement (red points) [45]. Inset figures show false-color plots of observed intensity distribution, in which the two-dimensional location of ZIP (white cross mark) is determined from the weighted-averaged position within 1% of the maximum intensity.

be directly determined by the ZIP from a single image of the intensity distribution. Figure 4 shows calculated fidelities between estimated polarization states from the weak measurement and prepared states determined by the angle θ [see Figs. 3(a) and 3(c)]. The averaged fidelity is calculated as 0.994. The measurement error is mainly attributed to the imperfection of the PSI setup and the mode conversion.

IV. SUMMARY AND DISCUSSION

In summary, we proposed a stereographical-visualization scheme for the qubit state by two-dimensional imaging of the weak value. We experimentally performed a single-setup weak measurement to evaluate the polarization state of photons using the LG mode. We also estimated the accuracy of our scheme from the fidelity of measurement results. Our approach to polarization measurement has the advantage in optics that we may extract information on the polarization from a single image, in cases of very small photon number, and in the characterization of polarization-entangled quantum states. By inferring the probability density of the polarization conditioned on *a priori* information, we can explore the implications of polarization measurements at very low light levels.

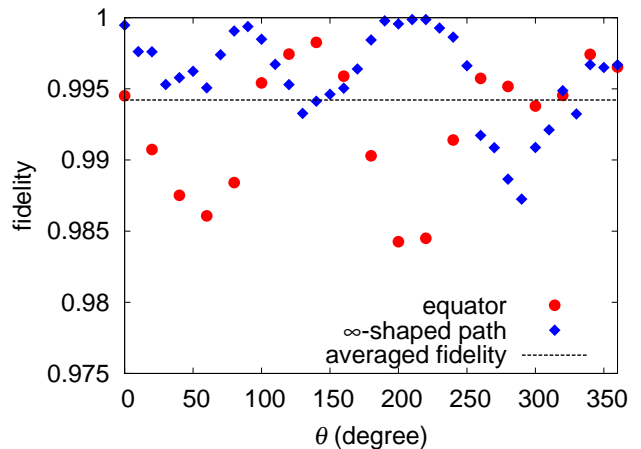


FIG. 4: Calculated fidelities of estimated states from the weak measurement with prepared states on the equator (red circles) and on the ∞ -shaped path (blue diamonds). Averaged fidelity is calculated as 0.994.

For a very small number of independent photons, our formalism suggests that each photon represents an individual stochastic event described by a spatial probability density function. However, the angle between the ZIP and our stereographic projection onto the

complex projective plane $\mathbb{CP}(1)$ of the quantum state is related to the fidelity via the Fubini–Study metric [41]. Further, the fidelity of the mixed state case [42] can be generalized via the Bures metric [43]. Therefore, the ZIP may directly visualize the geometrical structure of the quantum state, the Kähler manifold [44].

Acknowledgments

We thank Ian Wamsley, Andrew Briggs, George C. Knee, and Erik M. Gauger for providing useful comments and suggestions. This work was supported by a Grant for Basic Science Research Projects from The Sumitomo Foundation, a grant from Matsuo Foundation, IMS Joint Study Program, and JSPS KAKENHI Grants No. 25790068 and No. 25287101.

Appendix A: Exact calculation of weak measurement

In the main text, we use the weak measurement scheme under the approximation condition (weak condition);

$$\frac{W_0}{G} \gg \max(1, |\langle \hat{\sigma}_x \rangle_w|). \quad (\text{A1})$$

In what follows, the probe state is calculated without the weak condition under the same setup in the main text. The initial state of the probe state is set the LG beam with $l = 1$;

$$\phi_i(x, y) := N(x + iy) \exp\left(-\frac{x^2 + y^2}{4W_0^2}\right), \quad (\text{A2})$$

where N is the normalization constant. The probe state after the measurement interaction with taking the post-selection is

$$\phi_f(x, y) = \frac{\langle 1|\psi \rangle}{2} \left\{ (1 - \langle \hat{\sigma}_x \rangle_w) \phi_i(x + G, y) + (1 + \langle \hat{\sigma}_x \rangle_w) \phi_i(x - G, y) \right\}. \quad (\text{A3})$$

The above equation can be approximated under the weak condition as

$$\phi_f(x, y) \simeq \langle 1|\psi \rangle \phi_i(x - G \langle \hat{\sigma}_x \rangle_w, y) \quad (\text{A4})$$

Without the approximation, the average position of the intensity distribution is calculated as

$$\begin{aligned} \langle \hat{X} \rangle_f &= \frac{G \operatorname{Re} \langle \hat{\sigma}_x \rangle_w}{\frac{1}{2} \{1 + |\langle \hat{\sigma}_x \rangle_w|^2 + \eta(1 - |\langle \hat{\sigma}_x \rangle_w|^2)\}} \\ &= \frac{G \cos \phi \sin \theta}{1 - \eta \cos \theta} \\ &\xrightarrow{\text{weak condition}} G \operatorname{Re} \langle \hat{\sigma}_x \rangle_w \end{aligned} \quad (\text{A5})$$

$$\begin{aligned} \langle \hat{Y} \rangle_f &= \frac{G e^{-G^2/2W_0^2} \operatorname{Im} \langle \hat{\sigma}_x \rangle_w}{\frac{1}{2} \{1 + |\langle \hat{\sigma}_x \rangle_w|^2 + \eta(1 - |\langle \hat{\sigma}_x \rangle_w|^2)\}} \\ &= \frac{G e^{-G^2/2W_0^2} \sin \phi \sin \theta}{1 - \eta \cos \theta} \\ &\xrightarrow{\text{weak condition}} G \operatorname{Im} \langle \hat{\sigma}_x \rangle_w, \end{aligned} \quad (\text{A6})$$

where

$$\begin{aligned} |\psi \rangle &\equiv \cos \theta |0 \rangle + e^{i\phi} \sin \theta |1 \rangle, \\ \eta &\equiv \left(1 - \frac{G^2}{2W_0^2}\right) e^{-G^2/2W_0^2}. \end{aligned} \quad (\text{A7})$$

The results under the weak condition [(A5), (A6)] are the same as those in Refs. [19, 20].

-
- [1] Y. Aharonov, D. Z. Albert, and L. Vaidman, *Phys. Rev. Lett.* **60**, 1351 (1988).
[2] Y. Aharonov, P. G. Bergmann, and J. L. Lebowitz, *Phys. Rev.* **134**, B1410 (1964).
[3] Y. Aharonov and D. Rohrlich, *Quantum Paradoxes* (Wiley-VCH, Weinheim, 2005).
[4] Y. Aharonov and L. Vaidman, in *Time in Quantum Mechanics*, Vol. 1, edited by J. G. Muga, R. Sala Mayato, and I. L. Egusquiza (Springer, Berlin Heidelberg, 2008), p. 399.
[5] Y. Aharonov and J. Tollaksen, in *Visions of Discovery: New Light on Physics, Cosmology, and Consciousness*, edited by R. Y. Chiao, M. L. Cohen, A. J. Leggett, W. D. Phillips, and C. L. Harper, Jr. (Cambridge University Press, Cambridge, 2011), p. 105.
[6] Y. Shikano, in *Measurements in Quantum Mechanics*, edited by M. R. Pahlavani (InTech, Rijeka, Croatia, 2012), p. 75, arXiv:1110.5055.
[7] J. Dressel, M. Malik, F. M. Miatto, A. N. Jordan, and R. W. Boyd, *Rev. Mod. Phys.* **86**, 307 (2014).
[8] H. F. Hofmann, *Phys. Rev. A* **81**, 012103 (2010).
[9] S. Massar and S. Popescu, *Phys. Rev. A* **84**, 052106 (2011).
[10] S. Wu, *Sci. Rep.* **3**, 1193 (2013).
[11] A. Di Lorenzo, *Phys. Rev. A* **88**, 042114 (2013).
[12] L. Maccone and C. C. Rusconi, *Phys. Rev. A* **89**, 022122

- (2014).
- [13] J. B. Altepeter, D. F. V. James, and P. G. Kwiat, *Lect. Notes Phys.* **649**, 113 (2004).
- [14] J. S. Lundeen, B. Sutherland, A. Patel, C. Stewart, and C. Bamber, *Nature (London)* **474**, 188 (2011).
- [15] S. Kocsis, B. Braverman, S. Ravets, M. J. Stevens, R. P. Mirin, L. K. Shalm, and A. M. Steinberg, *Science* **332**, 1170 (2011).
- [16] B. Braverman and C. Simon, *Phys. Rev. Lett.* **110**, 060406 (2013).
- [17] J. Z. Salvail, M. Agnew, A. S. Johnson, E. Bolduc, J. Leach, and R. W. Boyd, *Nat. Photonics* **7**, 316 (2013).
- [18] M. Malik, M. Mirhosseini, M. P. Lavery, J. Leach, M. J. Padgett, and R. W. Boyd, *Nat. Commun.* **5**, 3115 (2014).
- [19] G. Puentes, N. Hermosa, and J. P. Torres, *Phys. Rev. Lett.* **109**, 040401 (2012).
- [20] H. Kobayashi, G. Puentes, and Y. Shikano, *Phys. Rev. A* **86**, 053805 (2012).
- [21] J. Nye and M. Berry, *Proc. R. Soc. London, Ser. A* **336**, 165 (1974).
- [22] V. Y. Bazhenov, M. Vasnetsov, and M. Soskin, *JETP Lett.* **52**, 429 (1990).
- [23] A. G. White, C. P. Smith, N. R. Heckenberg, H. Rubinsztein-Dunlop, R. McDuff, C. O. Weiss, and C. Tamm, *J. Mod. Opt.* **38**, 2531 (1991).
- [24] N. R. Heckenberg, R. McDuff, C. P. Smith, and A. G. White, *Opt. Lett.* **17**, 221 (1992).
- [25] L. Allen, M. W. Beijersbergen, R. J. C. Spreeuw, and J. P. Woerdman, *Phys. Rev. A* **45**, 8185 (1992).
- [26] M. Beijersbergen, R. Coerwinkel, M. Kristensen, and J. Woerdman, *Opt. Commun.* **112**, 321 (1994).
- [27] L. Marrucci, C. Manzo, and D. Paparo, *Phys. Rev. Lett.* **96**, 163905 (2006).
- [28] T. Ando, Y. Ohtake, N. Matsumoto, T. Inoue, and N. Fukuchi, *Opt. Lett.* **34**, 34 (2009).
- [29] M. Mansuripur, A. R. Zakharian, and E. M. Wright, *Phys. Rev. A* **84**, 033813 (2011).
- [30] H. Kobayashi, K. Nonaka, and M. Kitano, *Opt. Express* **20**, 14064 (2012).
- [31] M. R. Dennis and J. B. Götte, *New J. Phys.* **14**, 073013 (2012).
- [32] J. B. Götte and M. R. Dennis, *New J. Phys.* **14**, 073016 (2012).
- [33] M. R. Dennis and J. B. Götte, *Phys. Rev. Lett.* **109**, 183903 (2012).
- [34] J. B. Götte and M. R. Dennis, *Opt. Lett.* **38**, 2295 (2013).
- [35] O. S. Magaña-Loaiza, M. Mirhosseini, B. Rodenburg, and R. W. Boyd, arXiv:1312.2981.
- [36] J. Řeháček, B.-G. Englert, and D. Kaszlikowski, *Phys. Rev. A* **70**, 052321 (2004).
- [37] J. Nunn, B. J. Smith, G. Puentes, I. A. Walmsley, and J. S. Lundeen *Phys. Rev. A* **81**, 042109 (2010).
- [38] P. B. Dixon, D. J. Starling, A. N. Jordan, and J. C. Howell, *Phys. Rev. Lett.* **102**, 173601 (2009).
- [39] N. W. M. Ritchie, J. G. Story, and R. G. Hulet, *Phys. Rev. Lett.* **66**, 1107 (1991).
- [40] G. J. Pryde, J. L. O'Brien, A. G. White, T. C. Ralph, and H. M. Wiseman, *Phys. Rev. Lett.* **94**, 220405 (2005).
- [41] A. Uhlmann, *Rep. Math. Phys.* **9**, 273 (1976).
- [42] R. Jozsa, *J. Mod. Opt.* **41**, 2315 (1994).
- [43] C. A. Fuchs, Ph.D. thesis, University of New Mexico, 1995, arXiv:quant-ph/9601020.
- [44] I. Bengtsson and K. Życzkowski, *Geometry of Quantum States* (Cambridge University Press, Cambridge, 2006).
- [45] The weak interaction inside the PSI induces $240\mu\text{m}$ -deflection on the observation plane between the horizontally-polarized and vertically-polarized components. From this deflection value, the two-dimensional location of the ZIP is calibrated to the size of the Poincaré sphere.